Electronic Supporting Information

Versatile Electrochemical Manufacturing of Mixed Metal Sulfide /N-doped rGO Composites as Bifunctional Catalysts for High Power Rechargeable Zn-Air Batteries

Microstructural Characterisation

Scanning electron microscopy (SEM) and energy dispersive X-ray (EDS spectrometry (EDS) were used to investigate the microstructure and composition of the coatings deposited onto the GF. SEM images of the samples were collected using a JEOL JSM-7900F with an energy-dispersive X-ray spectroscopy detector (X-EDS) Ultim Max 170 Oxford Instruments model. The microstructure of the materials was also studied by (scanning) transmission electron microscopy (TEM/STEM). TEM images were measured on a TEM JEOL 2100 instrument at an accelerating voltage of 200 kV. Crystal structure of the samples was analyzed by X-ray diffraction (XRD, PANalytical Empyream diffractometer) using Cu K_α radiation (λ=1.54178 Å) with a step size of 0.2 $°s^{-1}$, generated at 45 kV and an emission current of 40 mA. Thermo-gravimetric analysis (TGA) of the samples between 25–700 °C was performed using a TA Instruments SDT-Q600 analyser (heating rate of 10 °C min^{-1}). The specific surface area and pore size distribution of the samples were also measured following the multipoint Brunauer–Emmett–Teller (BET) and Barret–Joyner–Halenda (BJH) analysis methods, respectively from N2 adsorption/desorption isotherms using Quantachrome QuadraSorb-S equipment. Raman spectra were acquired using a Raman microscope (Alpha300 R, WiTech) with an Nd:YAG laser (532 nm wavelength), an optical objective of 50X, and an integration time of 1 s. X-ray photoelectron spectroscopy (XPS) was conducted to analyze the surface chemical composition of the NCMS/NrGO sample. NAPXPS and XAS measurements were conducted at the HIPPIE

beamline at MAX IV with the connection of a SP-2000 Biologic potentiostat. The electrochemical cell employed a three-electrode setup with NCMS/NrGO-GF as the working electrode, Pt foil as the counter electrode, and Ag/AgCl as the reference electrode, with a 0.1 M KOH solution as the electrolyte. An accelerated degradation test (ADT) was performed in cyclic voltammetry mode with a scan rate of 100 mV/s for 1000 cycles, ranging from 1.2 to 1.6 V. A monochromatic Al Ka source was used as the soft X-rays photon source. All XPS and XAS data were collected and quantified using SPECS software.

Electrochemical Measurements

4 *mg* of the catalyst gently scratched from graphene foam manually and 4 *mg* of Vulcan carbon (VC) were mixed thoroughly and dispersed in 500 μl of N-Methyl-2-pyrrolidone (NMP) by sonicating the mixture for 30 *min* in an ultrasonic bath to achieve a homogenous ink. 3 μl of the catalyst ink was drop-casted on a glassy carbon electrode (GCE, ALS Co., Japan) yielding a deposit 3 *mm* in diameter (catalyst mass loading of ~ 0.338 $mg{\cdot}cm^{-2}$) and subsequently dried at 80 °C for ~ 30 *min*. Cyclic voltammetry was conducted in an electrochemical cell sealed with Teflon® cap using 0.1 M KOH electrolyte, modified GCE as the working electrode, Pt spring as counter and Saturated Calomel Electrode (SCE, Saturated KCl, ALS, RE-2BP) as reference electrode. All electrochemical measurements were conducted on a *Bio-Logic* (VMP3) multichannel station. Before conducting experiments, the electrolyte (0.1 M KOH) was saturated with pure oxygen or argon (control experiments) by bubbling the gas into the electrolyte for at least 30 *min*. In order to ensure gas saturation, purging was continued above the solution during measurements. Cyclic voltammograms were recorded at a scan rate of 20 $m\mathrm{V}{\cdot}s^{-1}$ after 5 cycles over a potential range of 0.2 to -0.8 V vs. SCE. Potentials in all electrochemical measurements were converted into the reversible hydrogen electrode (RHE) scale according to the following equation which stands in 0.1 M KOH:

$$E_{RHE} = E_{SCE} + 0.99\ \text{V} \quad \text{in 0.1 M KOH} \tag{1}$$

PtRuC 20% (*FuelCellStore*, USA) was employed as commercial ORR, OER and bifunctional catalysts, respectively for comparison.

Rotating Disk Electrode (RDE) Measurements

The modified GCE, prepared as above-mentioned, was scanned cathodically at a scan rate of 20 mV·s^{-1} with various rotating speeds from 400 to 2300 *r.p.m*. using an RRDE-3A (ALS Co., Ltd) apparatus. *Koutecky-Levich* theory was employed to interpret ORR kinetics and provide a mechanism for this reaction. Accordingly, the number of electrons transferred (n) was estimated on the basis of following equation: [1]

$$\frac{1}{J} = \frac{1}{J_L} + \frac{1}{J_K} = \frac{1}{B\omega^{1/2}} + \frac{1}{J_K} \tag{2}$$

where J is the experimental current density (mA·cm^{-2}), J_K is kinetic-limiting current density ($J_K = nFkC_{o_2}$), J_L is the diffusion-limiting current density, ω is the angular velocity, and B can be defined as follows:

$$B = 0.62nFC_{O_2}(D_{o_2})^{2/3}\nu^{-1/6} \tag{3}$$

where F is the Faraday constant (96,485 C·mol^{-1}), C_{O_2} is the bulk concentration of O_2 (1.15×10^{-6} $mol{\cdot}cm^{-3}$ in 0.1 M KOH), $D_{o_2}$is the diffusion coefficient of O_2 (1.90×10^{-5} $cm^2{\cdot}s^{-1}$), and ν is the kinematic viscosity of the electrolyte (0.01 $cm^2{\cdot}s^{-1}$). For the *Tafel* plots, the kinetic current has been estimated from the mass-transport correction of RDE using the following equation: [1]

$$J_K = \frac{(J \times J_L)}{(J_L - J)} \tag{4}$$

Rotating Ring-Disk Electrode (RRDE) measurements

The catalyst ink (4 *μl)*, prepared according to the above-mentioned recipe, was drop-cast on the surface of a glassy carbon disk (Pt ring/GC disk electrode, ALS Co., Ltd) yielding a deposit 4 *mm* in diameter. After drying at 80 °C for ~ 30 *min*, the disk electrode was scanned cathodically at a scan rate of 20 *m*V·s^{-1} while a constant potential of 1.49 V vs. RHE was applied to the ring electrode in 0.1 M KOH electrolyte. In such an experiment, the formation of peroxide (HO^{2-}) species on the disk electrode could be tracked by applying an oxidative potential to the ring electrode. Accordingly, a small ring current suggests that the reaction has gone through a 4*e* pathway. The number of electrons transferred, and percentage of peroxide formation were calculated according to:

$$n = 4 \times \frac{I_D}{I_D + \frac{I_R}{N}} \tag{5}$$

$$\%HO_2^- = 200 \times \frac{\frac{I_R}{N}}{I_D + \frac{I_R}{N}} \tag{6}$$

where I_D is disk current, I_R is ring current, and N is the current collection efficiency ($N = -I_R/I_D$) of the Pt ring electrode. N was measured by scanning GC disk electrode from 1.44 to 0.99 V vs. RHE at 20 *m*V·s^{-1} and applying a constant potential of 1.44 V to the ring electrode in an aqueous solution of 5 *m*M $K_3Fe[CN]_6$ and 0.1 M KCl.

Assembly of Zn-Air Battery Cells

Air cathodes were fabricated by coating firstly a thin layer of NrGO on GF using EPD to further enhance the adhesion and stability of the active material. Then, we used CED to deposit the NCMS on NrGO, forming an array of redox-active interconnected NCMS nanosheets. In such a structure, the NrGO sheets act both as nano-pillars to separate the sulfide nanosheets, which buffer the volume changes of the undergone sulfides, and as electrical connections to the

sulfides. The prepared electrodes were mounted in a 3D-printed designed cell with perforations on the cathode side, together with a Zn foil (Goodfellow, UK; purity: 99.9%; *1.25 cm^2*) as anode. The cell was filled with 6 M KOH and 0.2 M $ZnCl_2$ (~ 3 *ml*) solution as the electrolyte.

Density Functional Theory Calculations

Density Functional Theory calculations were conducted using the plane wave code, Vienna Ab Initio Simulation Package (VASP 6.2.0) by utilizing the all-electron projector augmented wave (PAW) method. [2] The electron exchange and correlations were defined using the generalized gradient approximation (GGA), while pseudo potentials were employed within the Perdew, Burke, and Ernzerhof (*PBE*) parametrization. [2] While modeling the catalyst surfaces along with graphene, rGO and N-rGO substrate features , a supercell approach was used such that sufficient vacuum layers (20 Å) were added along the Z direction to create the surface slabs while assuming infinite periodicity along X and Y directions. [3] The catalyst models created for this study mainly included NCMS/rGO and NCMS/N-rGO. For the Brillouin zone integration, Monkhorst pack K point grids of appropriate dimensions were used. Spin polarization was included, and the surfaces were adjusted with energy and force tolerance values of 1×10^{-6} eV and 1×10^{-3} eV $Å^{-1}$, respectively. The adsorption energies of O_2 and H_2O molecules on the surfaces of NCMS over rGO and NrGO, were calculated based on the following formula,

$$E_{ads} = E_{(surf + adsorbate)} - E_{(surf)} - E_{(adsorbate)} \quad (7)$$

Where, the first term on the RHS indicates the total energy of the graphene system with adsorbate, the second term represents the total energy of the corresponding surface without adsorbate, and last term is the total energy of the free-standing adsorbate respectively. Here the surfaces are rGO and NrGO with NCMS adsorbed on it and the oxygen and water molecules are adsorbed on the combined system.

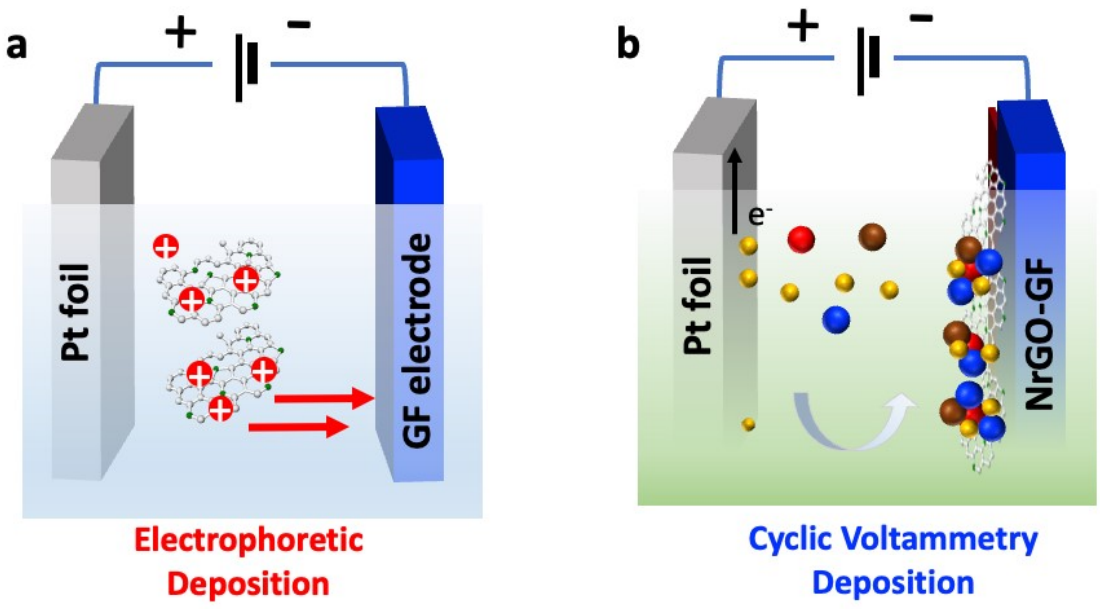

Scheme S1. Schematic illustration of the electrophoretic deposition and cyclic voltammetry deposition in a consecutive two-steps process.

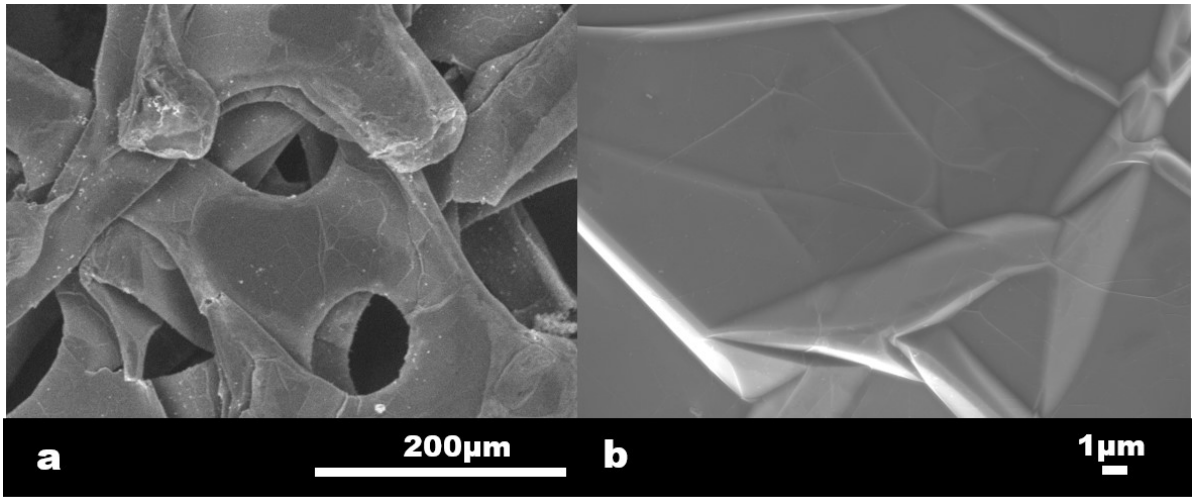

Figure S1. SEM images of the CVD Graphene Foam as a free-standing substrate.

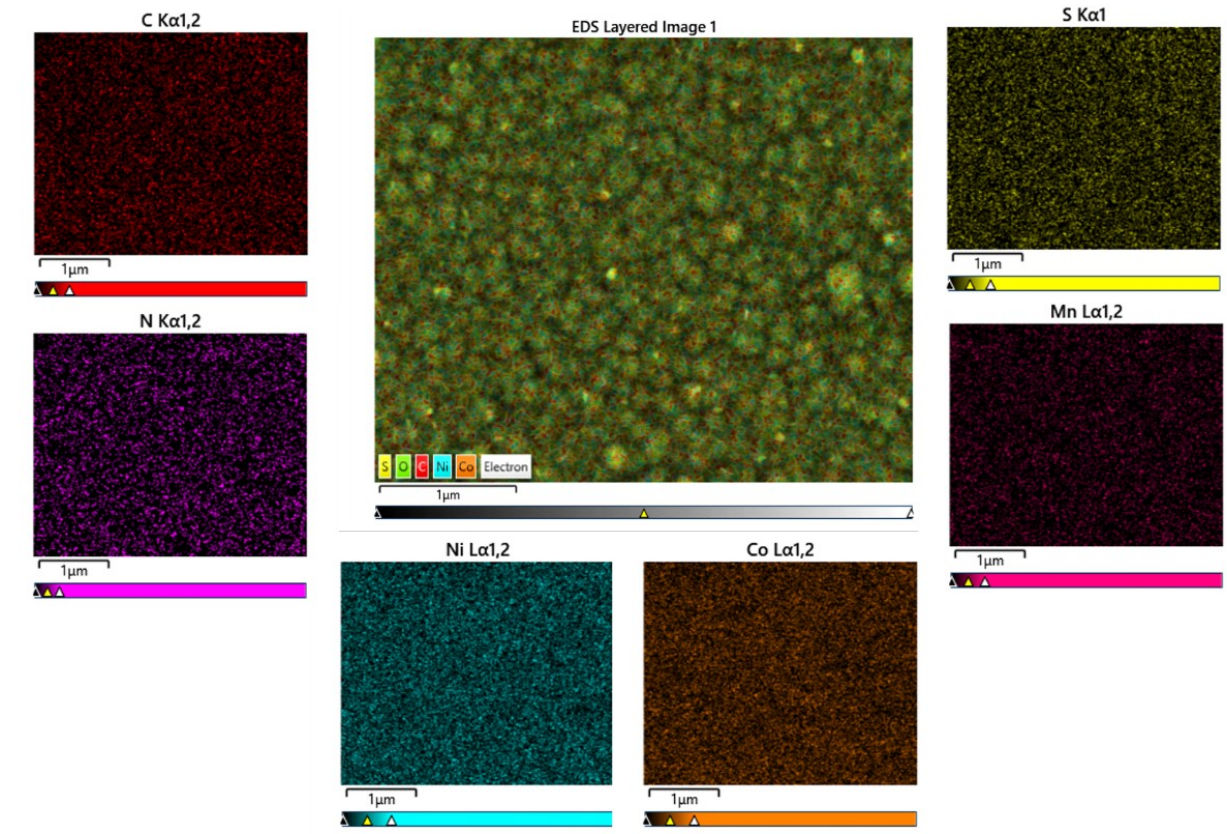

Figure S2. EDS Image and corresponding element mapping of C, N, Ni, Co, S and Mn on the NCMS/NrGO-GF sample

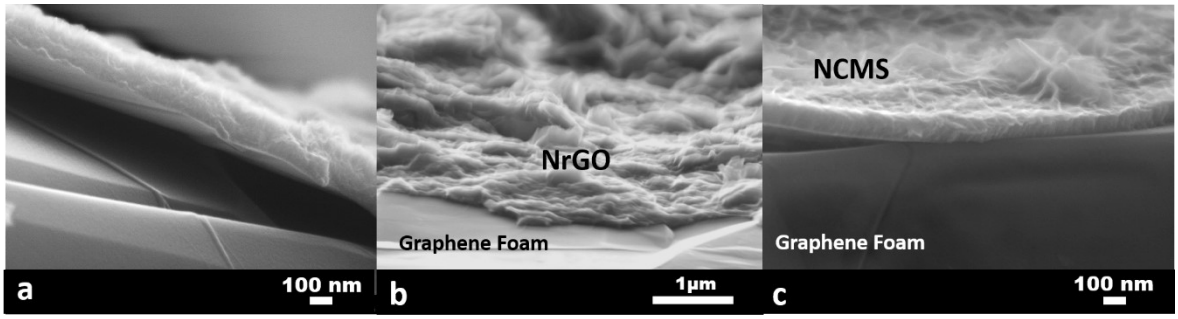

Figure S3. Cross-sectional SEM images of (a) NCMS/NrGO-GF (b) NrGO-GF (c) bulk NCMS (direct growth onto GF)

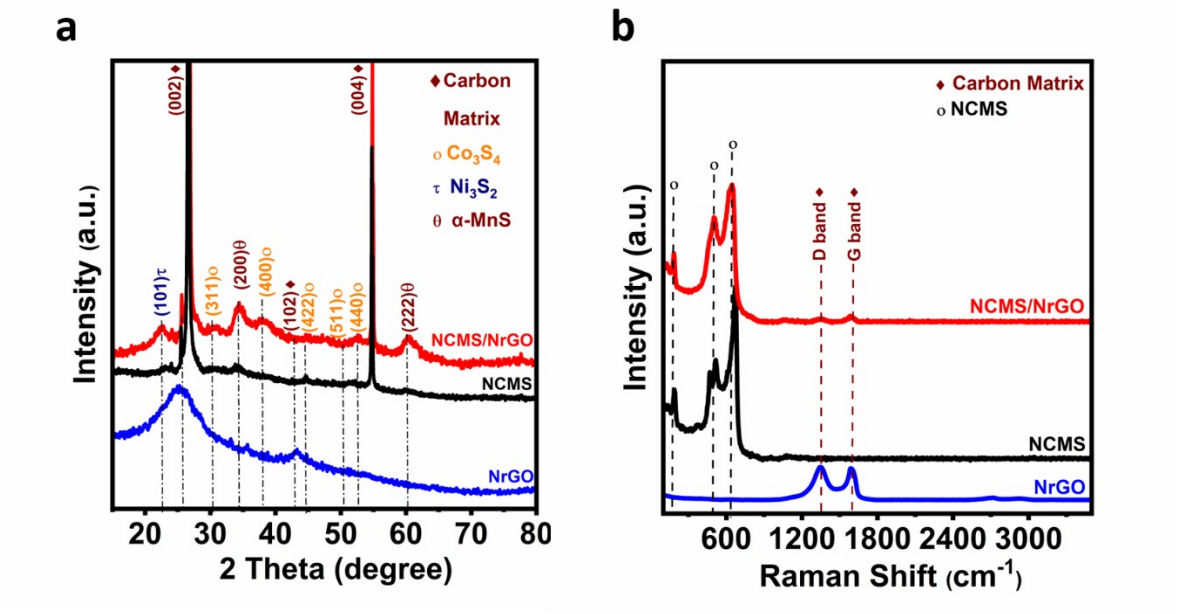

Figure S4. Microstructural analysis of the samples growth onto the GF: (a) XRD, (b) Raman spectroscopy.

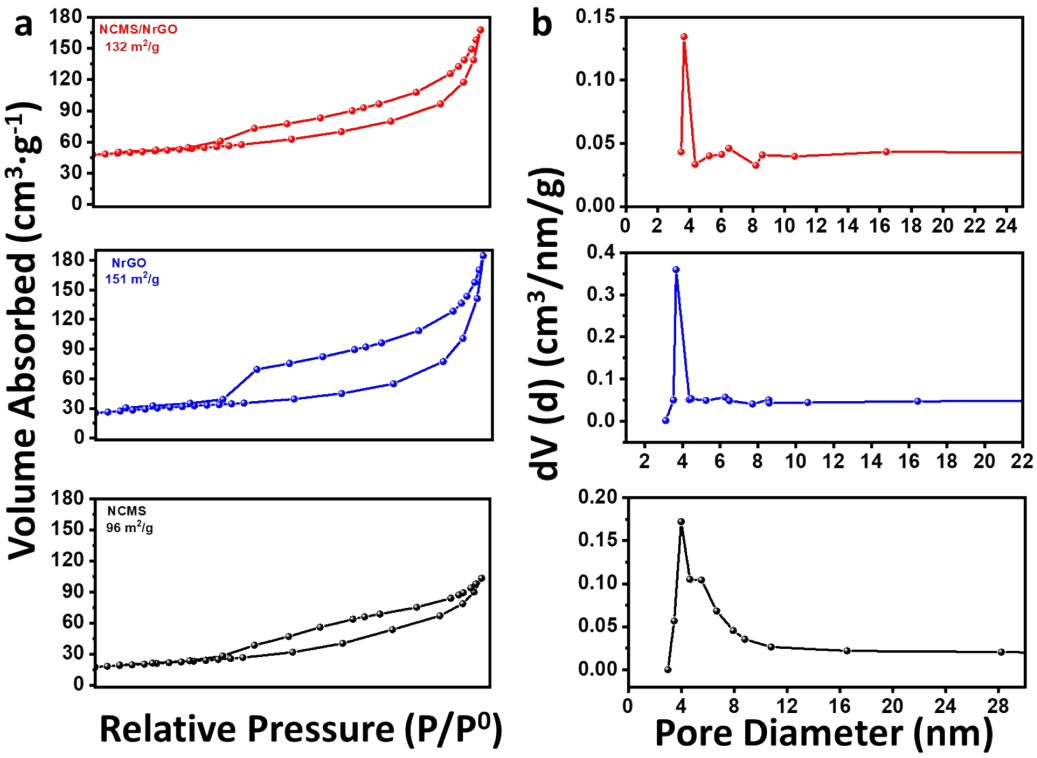

Figure S5. N2 adsorption-desorption isotherms and Pore size distribution of the different samples

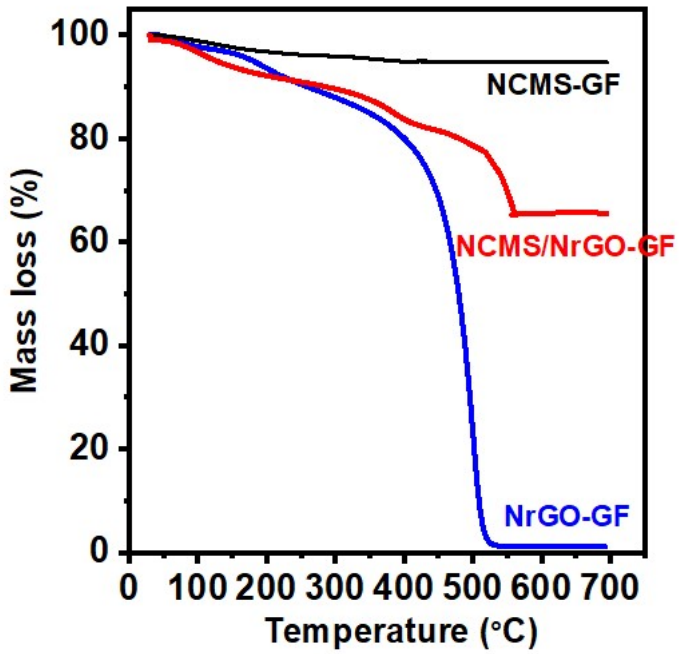

Figure S6. TGA profile of the samples from room temperature to 700 °C with a heating rate of 10 °C min^{-1} under air flow. The slow mass loss before 450 ºC is caused by the removal of water and hydroxy groups probably adsorbed on the surface of the samples. The continuous

weight loss from 450 ºC to 550 ºC is ascribed to the burning of graphene oxide since the temperature of thermal decomposition and oxidation of sulfide to oxide is above 650 ºC. Therefore, the weight compositions are 94.8 wt% and 65.5 wt%, in NCMS and NCMS/NrGO, respectively.

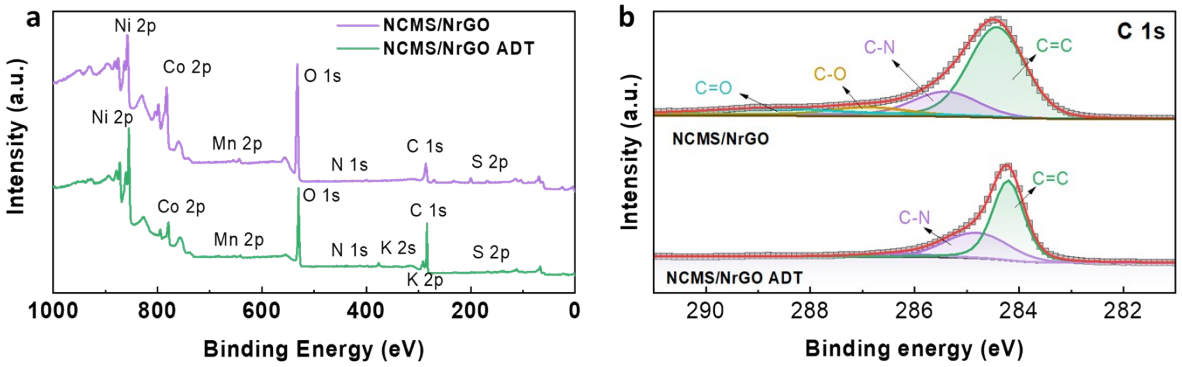

Figure S7. a) XPS full spectra and high-resolution spectra of C 1s of NCMS-NrGO before and after accelerated durability test (ADT).

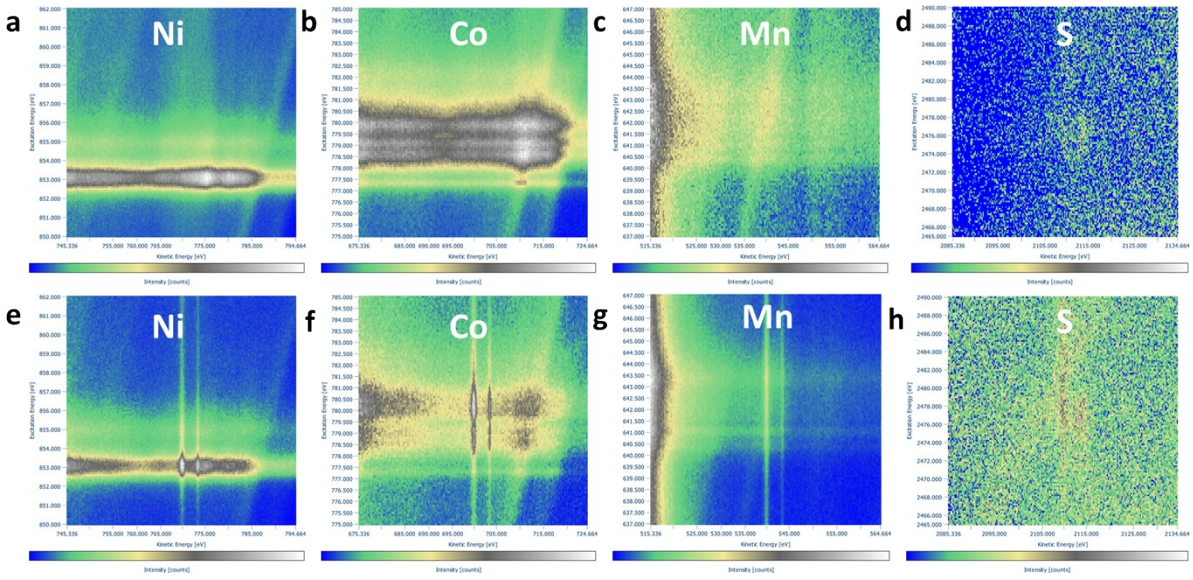

Figure S8. 2D Auger yield of Ni, Co, and Mn L-edge XAS spectra of NCMS-NrGO composites. a) Ni, b) Co, c) Mn L3-edge, d) S K-edge XAS data of NCMS-NrGO before accelerated durability test (ADT); e) Ni, f) Co, g) Mn L3 edge, h) S K-edge XAS data of NCMS-NrGO after ADT cycling. The two vertical bands at constant in Figure e-g) are an instrument artifact.

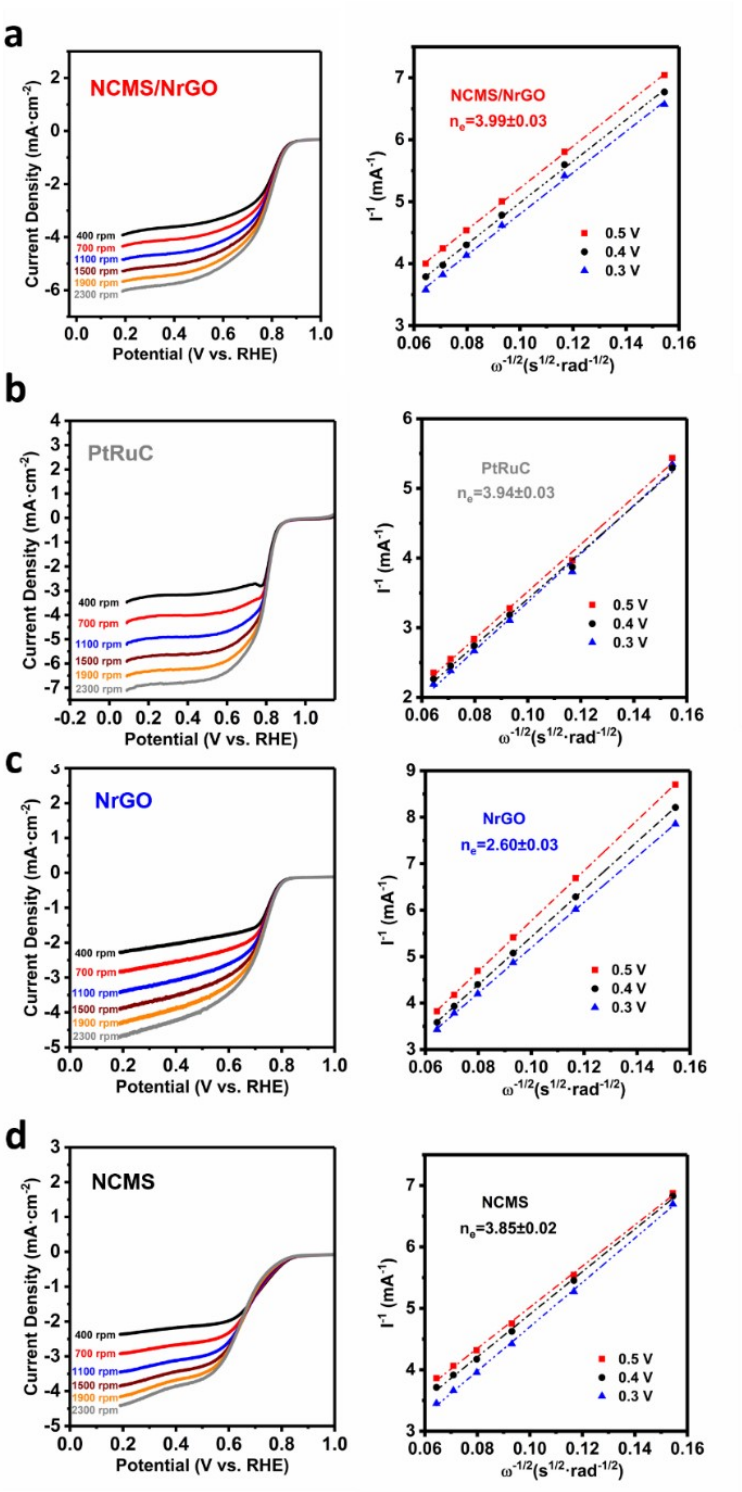

Figure S9. LSV curves of the samples at various rotation rates in O_2-saturated 0.1M KOH solution with a scan rate of 20 mV·s-1 and corresponding Koutechy-Levich plots (a) NCMS/NrGO (b) PtRuC (c) NrGO (d) NCMS.

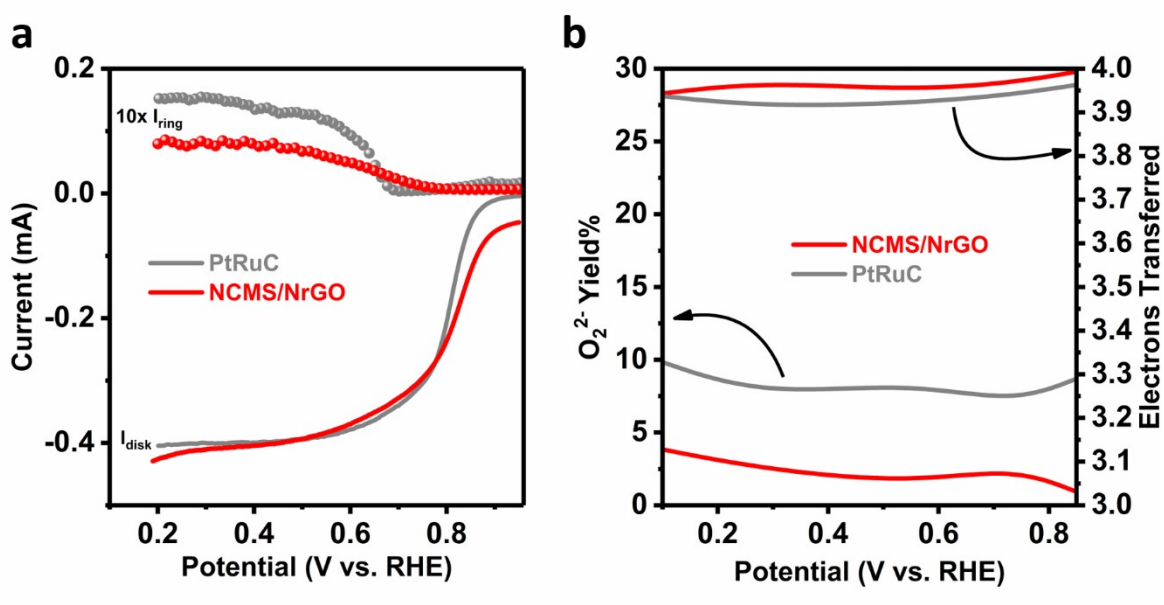

Figure S10. (a) RRDE LSV profiles and (b) corresponding percentage of peroxide and number of transferred electrons.

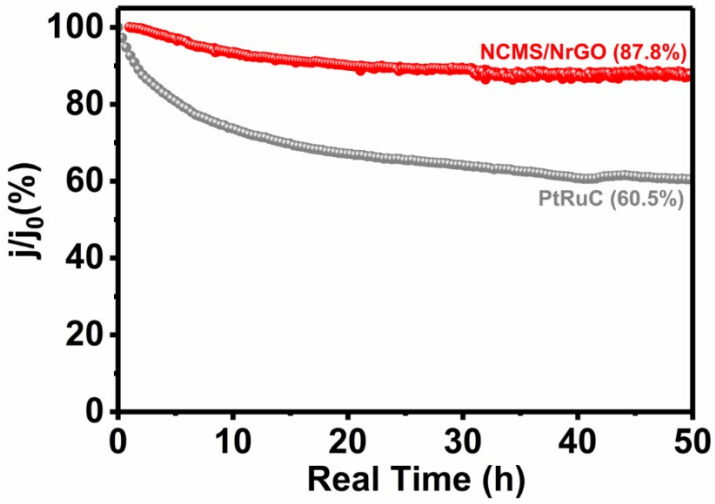

Figure S11. Durability of NCMS/NrGO and PtRuC catalysts towards ORR.

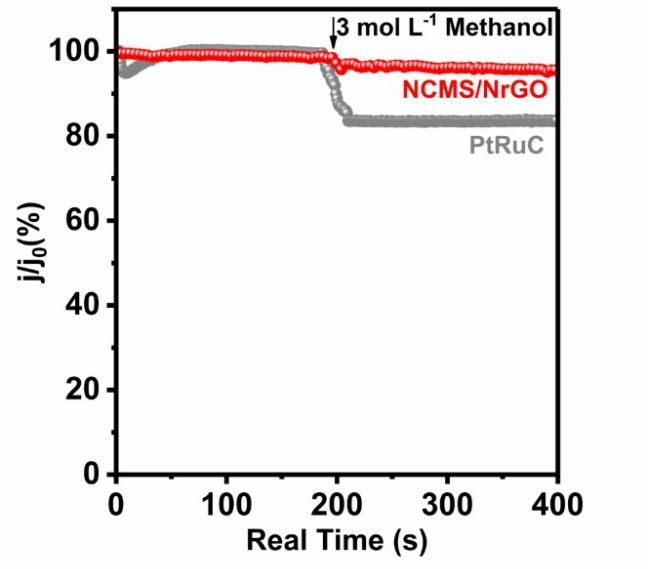

Figure S12. Methanol-crossover tests performed by adding methanol into the electrolyte at 200 s.

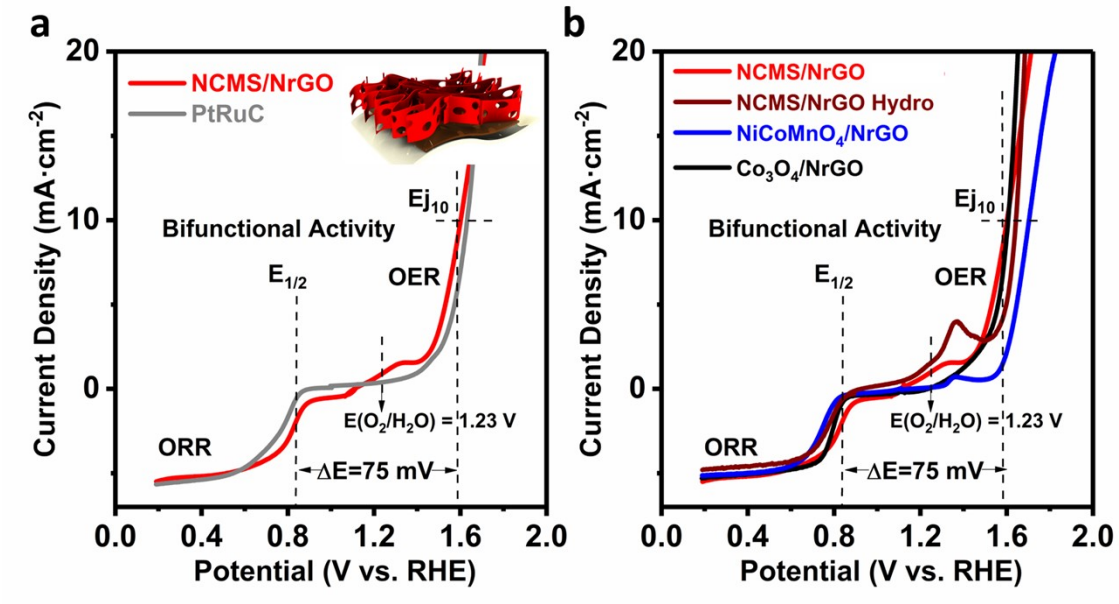

Figure S13. Entire LSV curves at 1500 rpm for bifunctional activities within the ORR and OER potential window of NCMS/NrGO developed in this work in comparison with (a) PtRuC catalyst (b) NCMS/NrGO, $NiCoMnO_4$/NrGO and Co_3O_4/NrGO synthesized by hydrothermal methods. [4-6]

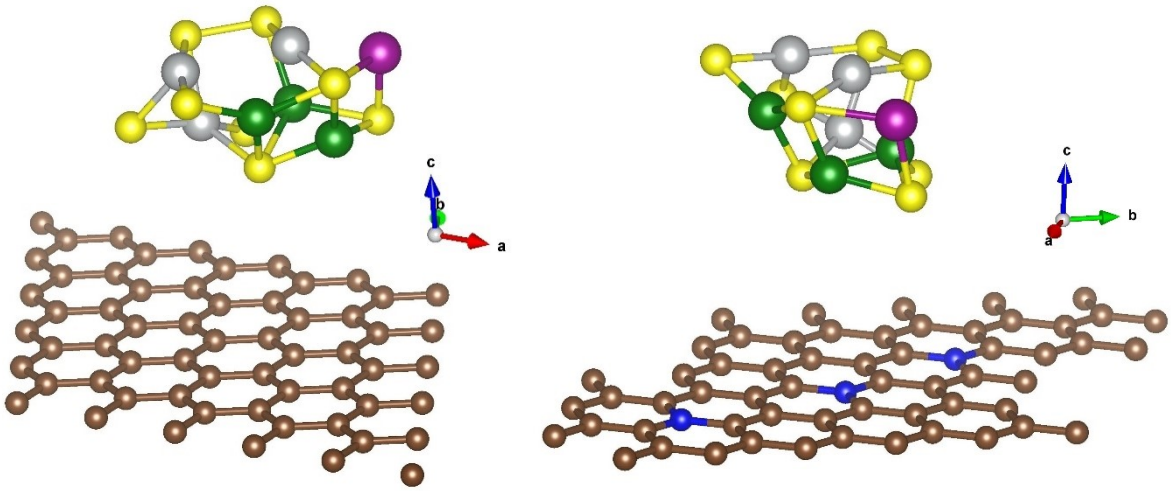

Figure S14. (a) NCMS cluster over rGO and (b) NCMS cluster over N-rGO

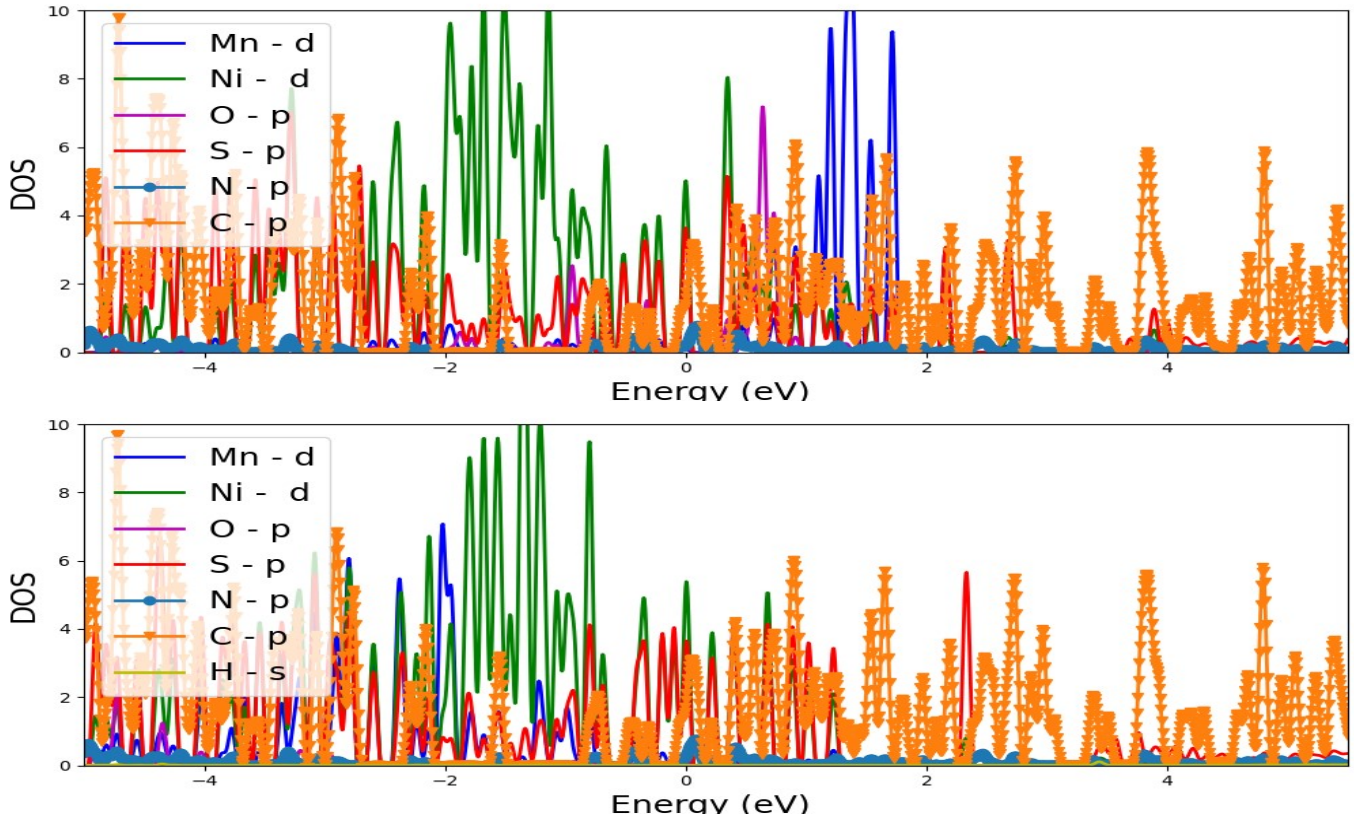

Figure S15. Density of states of for NCMS/NrGO during (a) O_2 adsorption and (b) H_2O adsorption

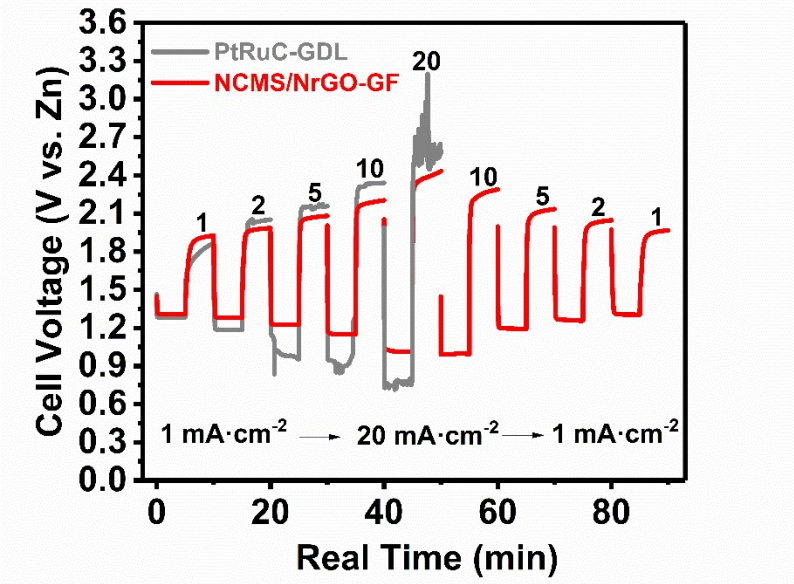

Figure S16. Study of the rechargeable Zn-air cells based on NCMS/NrGO-GF and PtRuC-GDL in charge conditions at different current densities.

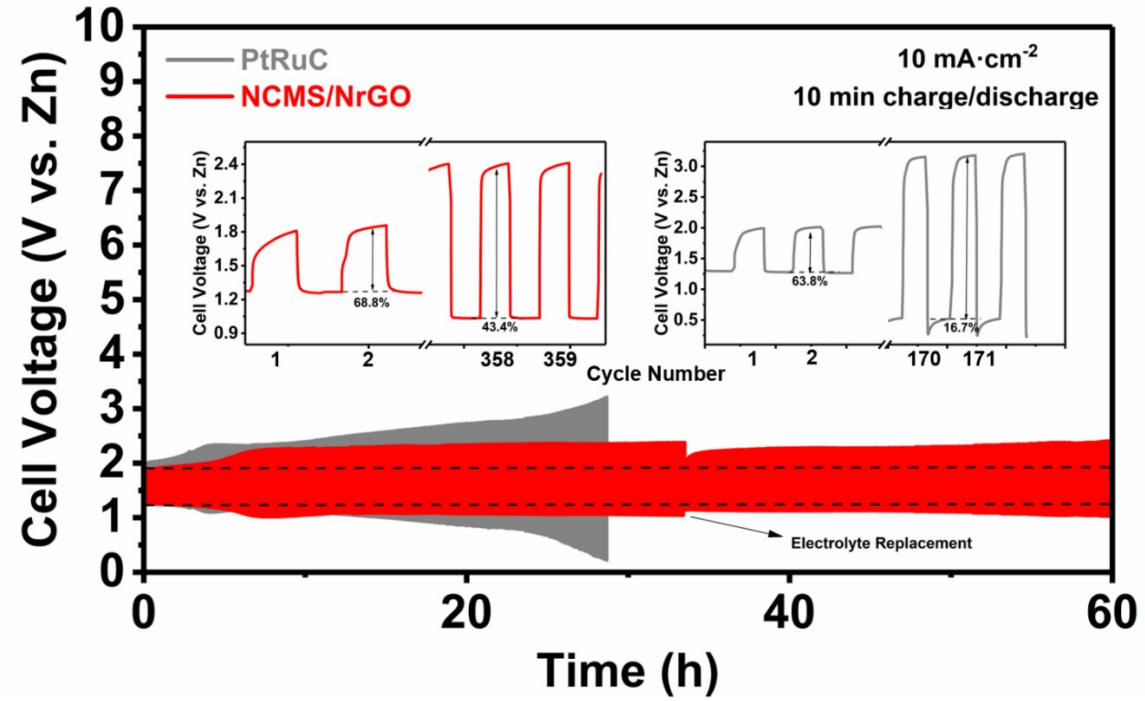

Figure S17. Cycling stability of rechargeable Zn-air cells based on NCMS/NrGO-GF and PtRuC-GDL as air cathode at 10 mA cm^{-2}. Inset shows 1st and last charge/discharge cycles of the NCMS/NrGO-GF and PtRuC for comparison.

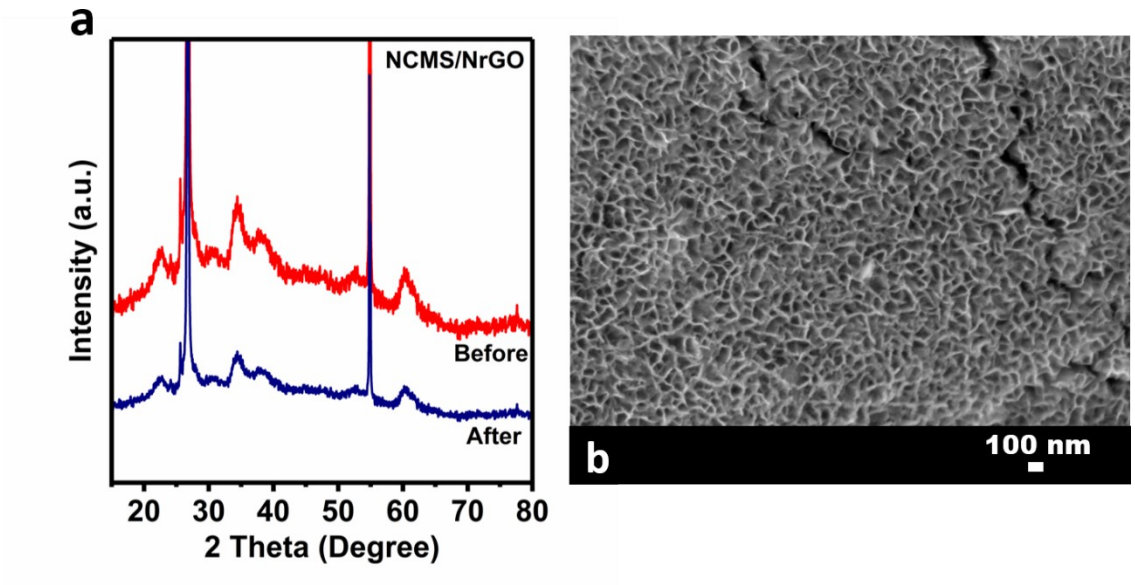

Figure S18. Post mortem analysis of the catalyst before and after cycling test at 2 mA.cm^{-2} (a) XRD (b) SEM.

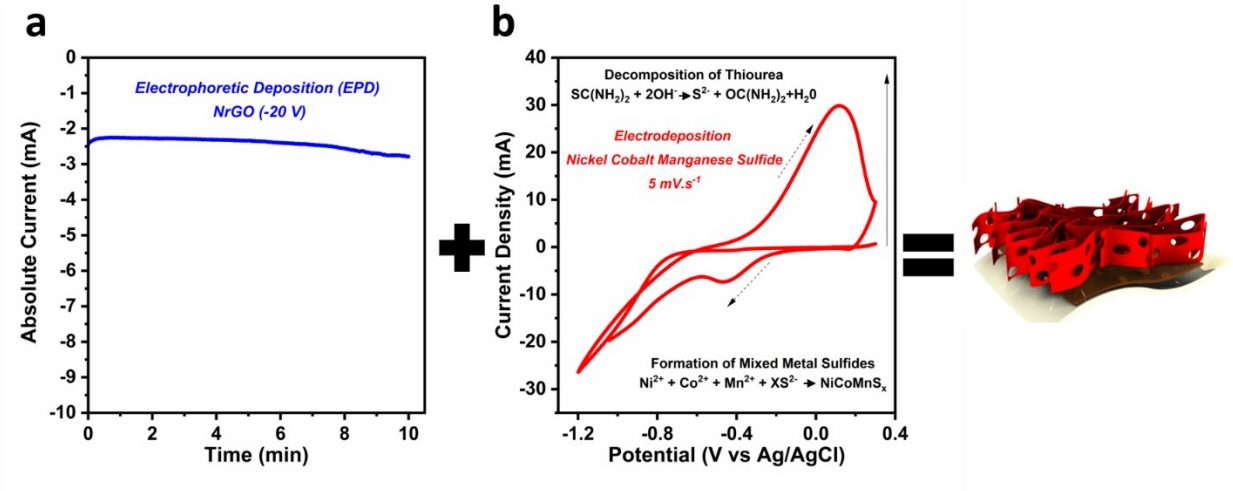

Figure S19. a) Electrophoretic deposition (EPD) of NrGO on GF b) cathodic electrodeposition of NCMS on top of a) via CV from water/EtOH co-solvent solution.

Table S1. Electrochemical parameters extracted from LSV curves in Figure 3b and comparison with recently reported non-noble metal catalysts in ORR.

Sample	E_{onset} (V vs. RHE)	$E_{1/2}$ (V vs. RHE)	J_{Levich} ($mA.cm^{-2}$)	Ref.
NCMS/NrGO	**0.94**	**0.83**	**5.51**	**This work**
NCMS	0.82	0.69	3.9	
NrGO	0.81	0.72	3.9	
PtRuC	0.89	0.79	5.61	
NCMS/NrGO	0.94	0.81	4.98	[5] Energy Storage Materials (2019)
Co_3O_4/NrGO	0.91	0.80	5.31	[7] Catalysis Science & Technology (2020)
$NiCo_2S_4$@g-C_3N_4-CNT	0.87	0.76	4.8	[8] Advanced Materials (2019)
$NiCo_2S_4$/NCNT	0.93	0.80	3.20	[9] Nano Energy (2017)
Nd/Co@NC	1.03	0.85	-	[16] Adv. Energy Mater. (2023)
Co@Tb_2O_3/NC	1.02	0.85	-	[17] Energy Environ. Sci. (2023)
$NiCo_2S_4$@NiFe LDH	0.97	0.85	4.49	[10] Applied Catalysis B: Environmental (2021)
$NiCo_2S_4$	0.89	0.80	4.21	
NiFe LDH	0.85	0.67	1.47	

Table S2. DFT calculation results of the bond length of O_2 adsorbed on NCMS/NrGO sites during ORR.

	Binding energy	Distance from surface
O_2 - Ni	**-1.75 eV**	Ni - O (of O_2) – **1.87 Å**
O_2 - S	**-1.18 eV**	S - O – **3.59 Å**

Table S3. DFT calculation results of the bond length of H_2O adsorbed on NCMS/NrGO sites during OER.

	Binding energy	Distance from surface
H_2O - Ni	**-0.464 eV**	Ni - O (of H_2O) – **2.10 Å**
H_2O – Co (after relaxation it was attached to Ni)	**-0.415 eV**	Ni-O – **2.14 Å**

H_2O – Mn	**-1.10 eV**	Mn-O - **2.16 Å**
H_2O - S	**5.81 eV**	S -O – **1.44 Å**

Table S4. Comparison of the performance of Zn-air batteries made with NCMS/NrGO hybrid as oxygen electrode catalysts with recently reported mixed metal compound electrocatalysts.

Electrocatalyst	Synthesis Method	Mass Loading ($mg.cm^{-2}$)	Electrolyte (Substrate)	Capacity ($mAh.g_{Zn}^{-1}$)	Max. Energy Density ($Wh.Kg^{-1}$)	OCV (V)	Max. Power Density ($mW.cm^{-2}$)	Cycling Stability (h)	Ref.
NCMS/NrGO	**Electrosynthesis (Room Temperature)**	**1.0**	**6M KOH+ 0.2 $ZnCl_2$ Graphene Foam (GF)**	**815.5 at 10 $mA.cm^{-2}$**	**1001.4**	**1.42**	**124**	**260 at 2 $mA.cm^{-2}$**	**This work**
NCMS/NrGO	Reflux+ Hydrothermal (180ºC,5h)	0.6	6M KOH+ 0.02M $ZnSO_4$ Gas Diffusion Layer (GDL)	834 at 5 $mA.cm^{-2}$	959	1.41	56	30 at 2 $mA.cm^{-2}$	[5] (2019) Energy Storage Materials
Co_3O_4/NrGO	2 Hydrotermal (150ºC,6h) (180ºC,3h) + Annealing (500ºC,2h)	-	6M KOH+ 0.02M $ZnSO_4$ (GDL)	875 at 5 $mA.cm^{-2}$	1115	1.49	47	160 at 2 $mA.cm^{-2}$	[7] (2020) Catalysis Science & Technology
$NiCo_2S_4$@g-C_3N_4-CNT	2 Hydrothermal (80ºC,20h) (170ºC,3h) + Vacuum Filtration	2.3	6M KOH+ 0.2 $ZnCl_2$	485 at 10 $mA.cm^{-2}$	-	1.45	142	110 at 10 $mA.cm^{-2}$	[8] (2019) Advanced Materials
$NiCo_2S_4$/NCNT	Solvothermal (170ºC,3h)	1.0	6M KOH+ 0.2 $ZnCl_2$ (Carbon Fiber Paper)	431 at 10 $mA.cm^{-2}$	554.6	1.49	147	150 at 10 $mA.cm^{-2}$	[11] (2017) Nano Energy
Co_p@CoNC	Pyrolysis (900ºC,2h)	1.0	6M KOH+ 0.2 $Zn(Ac)_2$ (Carbon Paper)	794.1 at 10 $mA.cm^{-2}$	-	1.46	188	360 at 10 $mA.cm^{-2}$	[12] (2022) Energy Storage Materials
CoFe/S-N-C	2 Pyrolysis (550ºC,4h) (850ºC,2h)	1.0	6M KOH+ 0.2 $Zn(Ac)_2$ (Carbon Paper)	814 at 10 $mA.cm^{-2}$	1025	1.48	120	100 at 10 $mA.cm^{-2}$	[13] (2022) Chemical Engineering Journal
FeCoNC/D	Hydrothermal (200ºC,6h)+ Pyrolysis (750ºC,1h)	1.0	6M KOH+ 0.2 $Zn(Ac)_2$ (GDL)	725 at 10 $mA.cm^{-2}$	-	1.48	157	40 at 10 $mA.cm^{-2}$	[14] (2022) Applied Catalysis B: Environmental
Fe−Co−Ni MOF	Electrosynthesis (Room Temperature)	1.0	ZnO saturated 6.0 M KOH	733 at 5 $mA.cm^{-2}$	945	1.42	161	130 at 5 $mA.cm^{-2}$	[15] (2022) J. Am. Chem. Soc.
Nd/Co@NC	ZIF precusor synthesis (60ºC, 12h drying) + pyrolysis (700ºC, 1h)	-	11.25 M KOH + 0.5 M ZnO	-	-	1.36	70.6	24	[16] Adv. Energy Mater. (2023)
Co@Tb_2O_3/NC	Hydrotermal (200ºC,10h) + pyrolysis (800ºC,3h)	-	6M KOH+ 0.2 $Zn(Cl)_2$	782.8 at 5 $mA.cm^{-2}$	994.1	1.44	166	241.3 at 5 $mA.cm^{-2}$	[17] (2023) Energy Environ. Sci.
Pt-Gd_2O_3/C +RuO_2	Carbonation (800ºC,3h)	-	6M KOH+ 0.2 $Zn(Cl)_2$	724 at 5 $mA.cm^{-2}$	926.7	1.46	111.1	190 at 5 $mA.cm^{-2}$	[18] (2023) Agnew. Chem. Int. Ed.

Table S5. Surface chemical composition of NCMS/NrGO by XPS.

Sample	Element composition (atomic %)						
	Ni 2p	Co 2p	Mn 2p	S 2p	O 1s	C 1s	N 1s
NCMS/NrGO-GF	9.59	8.63	1.02	1.11	51.71	27.18	0.77

REFERENCES

[1] Y. Liang, Y. Li, H. Wang, J. Zhou, J. Wang, T. Regier, H. Dai, *Nat Mater* **2011**, 10, 780.

[2] G. Kresse, J. Hafner, *Journal of Physics-Condensed Matter* **1994**, 6, 8245.

[3] H. J. Monkhorst, J. D. Pack, *Physical Review B* **1976**, 13, 5188.

[4] A. Pendashteh, J. Palma, M. Anderson, R. Marcilla, *Applied Catalysis B: Environmental* **2017**, 201, 241.

[5] A. Pendashteh, J. S. Sanchez, J. Palma, M. Anderson, R. Marcilla, *Energy Storage Materials* **2019**, 20, 216.

[6] J. S. Sanchez, R. R. Maca, A. Pendashteh, V. Etacheri, V. A. D. O'Shea, M. Castillo-Rodriguez, J. Palma, R. Marcilla, *Catalysis Science & Technology* **2020**, 10, 1444.

[7] J. S. Sanchez, R. R. Maça, A. Pendashteh, V. Etacheri, V. A. de la Peña O'Shea, M. Castillo-Rodríguez, J. Palma, R. Marcilla, *Catalysis Science & Technology* **2020**, 10, 1444.

[8] X. Han, W. Zhang, X. Ma, C. Zhong, N. Zhao, W. Hu, Y. Deng, *Adv Mater* **2019**, 31, e1808281.

[9] X. P. Han, X. Y. Wu, C. Zhong, Y. D. Deng, N. Q. Zhao, W. B. Hu, *Nano Energy* **2017**, 31, 541.

[10] X. Feng, Q. Jiao, W. Chen, Y. Dang, Z. Dai, S. L. Suib, J. Zhang, Y. Zhao, H. Li, C. Feng, *Applied Catalysis B: Environmental* **2021**, 286.

[11] X. Han, X. Wu, C. Zhong, Y. Deng, N. Zhao, W. Hu, *Nano Energy* **2017**, 31, 541.

[12] H. Yang, S. Gao, D. Rao, X. Yan, *Energy Storage Materials* **2022**, 46, 553.

[13] G. Li, Y. Tang, T. Fu, Y. Xiang, Z. Xiong, Y. Si, C. Guo, Z. Jiang, *Chemical Engineering Journal* **2022**, 429.

[14] K. Kim, K. Min, Y. Go, Y. Lee, S. E. Shim, D. Lim, S.-H. Baeck, *Applied Catalysis B: Environmental* **2022**, 315.

[15] F. Shahbazi Farahani, M. S. Rahmanifar, A. Noori, M. F. El-Kady, N. Hassani, M. Neek-Amal, R. B. Kaner, M. F. Mousavi, *J Am Chem Soc* **2022**, 144, 3411.

[16] C. Fan, X. Wang, X. Wu, Y. Chen, Z. Wang, M. Li, D. Sun, Y. Tang, G. Fu, Adv. Energy Mater. 2023, 13, 2203244.

[17] X. Wnag, J. Zhang, P. Wang, L. Li, H. Wang, D. Sun, Y. Li, Y. Tang, X. F. Lu, Y. Wang, G. Yu, Energy Environ. Sci. 2023, 16, 5500.

[18] S. Ning, M. Li, X. Wang, D. Zhang, B. Zhang, C. Wang, D. Sun, Y. Tang, H. Li, K. Sun, G. Fu, Angew. Chem. Int. Ed. 2023, 62, e202314565